

---

# **Analytic Prediction of the Pattern Tolerance Distribution in Linear Phased Arrays with Random Excitation Errors Using Probabilistic Interval Analysis**

**P. Rocca, N. Anselmi, A. Benoni, and A. Massa**

---

## Contents

1	Introduction	3
2	Mathematical Formulation	5

ELEDIA Research Center

---

# 1 Introduction

Modern wireless communications systems require antennas able to guarantee high-quality and reliable data links. In many practical applications, arrays generating patterns with high peak directivity and low sidelobes are necessary. Towards this aim, several strategies have been proposed and adopted to synthesise suitable values for the control points (i.e. amplifiers and phase shifters). However, real antenna systems are unavoidably affected by tolerances and errors due to the antenna realization and use, for example, manufacturing imprecisions, coupling effects, mechanical deformations, thermal drift, failures, and other kinds of nonidealities caused by the interactions with external agents. Such errors cause modifications of the radiated beam and performance degradation arises. It is then fundamental to assess their impact on the antenna “response” especially in the case of complex radiating systems, like phased arrays, widely employed in highly demanding and critical applications (e.g. monitoring, surveillance and control).

In the literature, the sensitivity analysis of antenna arrays has been dealt with different prediction approaches, based on either statistical methods or interval methods. Statistical approaches evaluate the average pattern performance and provide approximated formulas for the confidence boundaries. In this framework, simple statistical rules have been derived for the probability density function of the power pattern and its main parameters (e.g. mainlobe peak, sidelobe level and nulls) by exploiting the *central limit theorem*. Although well established, they present limitations, due to the a priori assumptions or/and approximations and have shown not always guaranteeing reliable confidence bounds in case of small/medium array sizes. To avoid such limitations, Monte Carlo methods have been proposed, but their application turns out being prohibitive for large arrays due to the huge and numerically intractable number of possible error configurations to be tested.

Instead, Interval techniques compute the bounds of the antenna response (e.g. the power pattern and its features) by modeling the uncertain variables as intervals. In this framework, an approach based on the Cauchy-Schwartz inequality has been proposed to predict the worst case bounds of the radiating beam pattern in presence of calibration errors and mutual coupling effects. A different strategy based on the math of *Interval Analysis* (IA) has been proposed for dealing with the sensitivity analysis of linear arrays with errors on amplitudes, or phases. Unlike statistical and Monte Carlo approaches, Interval Analysis allows to evaluate in a deterministic, exhaustive and analytic fashion the effects of manufacturing tolerance in the control points of the beamforming network on the radiation pattern. It needs no a priori information unless the knowledge of the extreme points of the input intervals, which are the only terms involved in the IA-based operations. Moreover, the reliability of the predicted bounds are guaranteed by the IA *Inclusion Theorem*. A further extension of the interval analysis tool has involved also mutual coupling effects. Recently, also a Minkowski-based Interval Analysis (IA-MS) approach has been proposed and successfully applied to planar arrays to mitigate bounds overestimation due to the “wrapping effect” related to the representation of the “interval numbers”. Other applications of the interval analysis framework to linear antenna arrays can be found. To predict the impact of small excitation amplitude uncertainty on the radiated array pattern, a Taylor expansion-based interval pattern analysis method have been developed, addressing the dependence problem of the the classical interval arithmetic, which may lead to an overestimation of the performance intervals. Instead, have proposed a matrix-based interval arithmetic method again for linear antenna array with excitations amplitude errors only.

---

However, each IA-based technique proposed in the literature seems to overestimate the interval bounds compared to the Monte Carlo approach. Although this overestimation is mainly linked with the limited number of possible error configuration tested, it also means that some portion of the interval power pattern are more probable than others.

In this work, an innovative Probabilistic Interval Analysis tool will be proposed taking into account linear phased arrays with both amplitude and phase excitation tolerances. The interval power pattern has been divided into regions and a confidence level for each region has been calculated. In such a way a new useful information has been recovered: for a linear phased array not only the interval bounds are known but it is also possible to say with which probability the pattern of a nonideal linear phased array could be in a specific region. Let us focus on the IA-MS approach, which appears to outperform the other state-of-art methods in case of phased arrays with both amplitude and phase errors. Until now, after the computation of the Minkowski Sum between the 2D interval phasors, only the magnitude of the result interval polygon has been considered. Nevertheless, the result polygon has also an its own shape, thus the errored power pattern are not uniformly distributed inside the interval bounds. To exploit also such information, the result phasor can be divided into regions, each region surface can be computed and a probability value can be deduced.

## 2 Mathematical Formulation

Let us consider a linear phased array of  $N$  isotropic elements, uniformly-spaced along the x-axis. The values of the nominal excitations of the array elements are defined as:

$$W_n = A_n e^{jB_n}, \quad n = 1, \dots, N \quad (1)$$

being  $A_n$  and  $B_n$  the nominal amplitude and phase coefficients for  $n$ -th element.

This antenna generates a nominal power pattern equal to:

$$P(u) = |AF(u)|^2 \quad (2)$$

where  $AF(u)$  is the nominal array factor, defined as:

$$AF(u) = \sum_{n=1}^N A_n e^{jB_n} e^{jkd(n-1)u} \quad (3)$$

where  $j = \sqrt{-1}$  is the complex variable,  $k = \frac{2\pi}{\lambda}$  the free-space wavenumber and  $\lambda$  the wavelength,  $d$  the inter-element spacing and  $u = \sin \theta$  being  $\theta \in [-\frac{\pi}{2}, \frac{\pi}{2}]$  is the angular direction.

Let the amplifiers/attenuators and the phase shifters of the beamforming network be characterized by known or measurable tolerances, thus the interval excitations have the following formula:

$$[W_n] = [A_n] e^{j[B_n]} \quad n = 1, \dots, N \quad (4)$$

where  $[A_n] = [A_n^{inf}, A_n^{sup}] = [A_n - \xi_n, A_n + \xi_n]$ ,  $n = 1, \dots, N$  and  $[B_n] = [B_n^{inf}, B_n^{sup}] = [B_n - \gamma_n, B_n + \gamma_n]$ ,  $n = 1, \dots, N$  represent the amplitude and phase excitation interval for the  $n$ -th element, respectively.  $\xi_n$  and  $\gamma_n$  are the corresponding uncertainties.

The interval extension of the ‘‘crisp’’ array factor function (3) is mathematically defined as:

$$[AF(u)] = \sum_{n=1}^N [A_n] e^{j[B_n]} e^{jkd(n-1)u} \quad (5)$$

To compute (5) by determining its bounds as a function of the endpoints of the excitations (i.e.,  $A_n^{inf}$ ,  $A_n^{sup}$  and  $B_n^{inf}$ ,  $B_n^{sup}$ ), different interval-based approaches can be applied. In the following, the IA-MS approach will be adopted. IA-MS does not define an analytic relationship for the lower and upper bounds, but it considers algorithmic procedures for their computation. Each complex interval excitation  $[W_n]$  can be represented as an interval phasor (Fig. 1) and the Minkowski Sum can be applied.

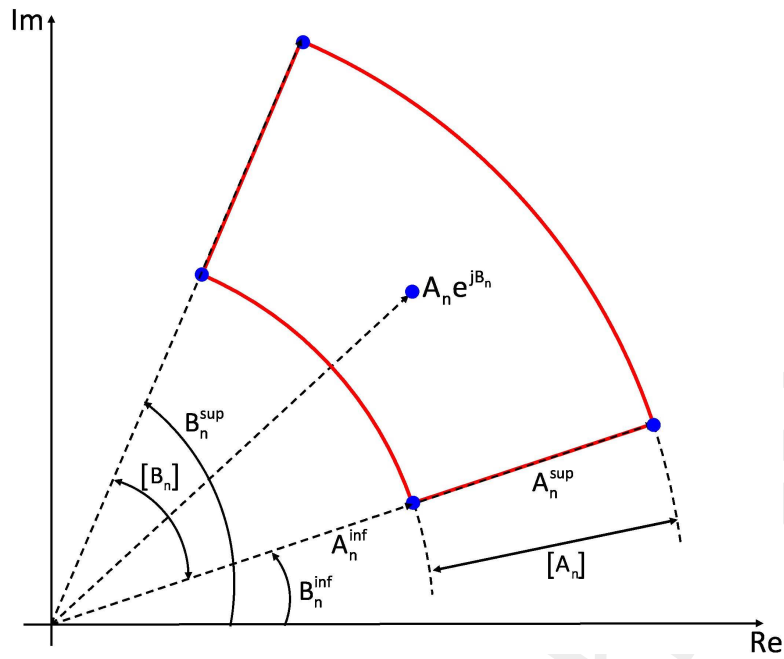


Figure 1: Complex-valued interval phasor  $[W_n]$ .

Thus, for each angular direction, according to the IA-MS method, a result interval polygon can be calculated. For the module of the IA-MS array factor  $[[AF(u)] = [|AF_{inf}(u)|, |AF_{sup}(u)|]]$ , the bounds are determined by selecting the minimum and the maximum distance with respect to the center of the complex plane as the left endpoint  $|AF_{inf}(u)|$  and the right endpoint  $|AF_{sup}(u)|$  (Fig. 2). Finally, the upper and lower bounds of  $[P(u)]$  are easily obtained as  $P_{inf}(u) = |AF_{inf}(u)|^2$  and  $P_{sup}(u) = |AF_{sup}(u)|^2$ , respectively.

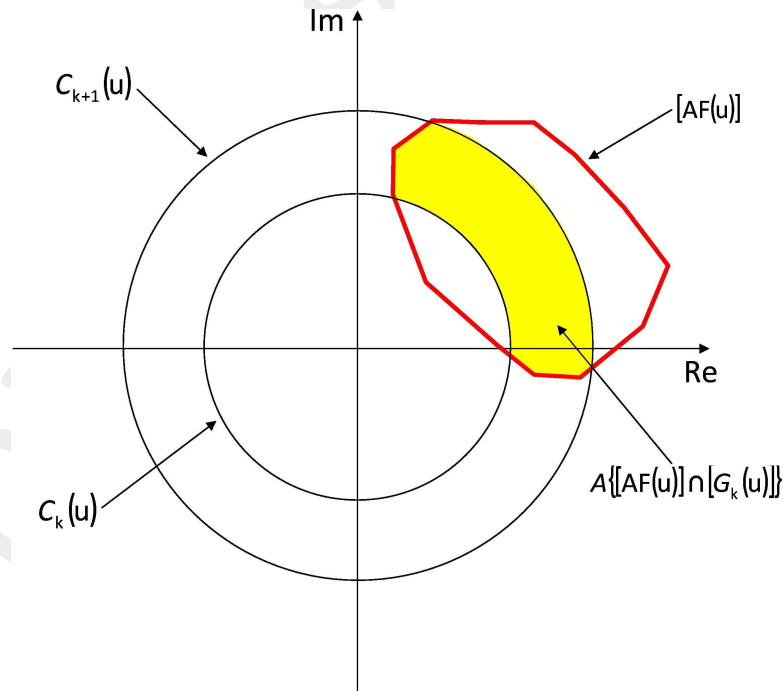


Figure 2: Array factor phasor  $[AF(u)]$  (red line), its module and width, and portion of annular region defined by  $|A_{inf}(u)|$  and  $|A_{sup}(u)|$  (light blue pattern).

Nevertheless, the result interval polygon  $[AF(u)]$ , obtained with the IA-MS method, contains more information than two

simple values, since the distribution of the possible random radiation pattern  $\hat{AF}(u)$  between the lower and upper bounds are not uniformly distributed. Therefore, it could be interesting to compute the probability for a given sample pattern  $\hat{AF}(u)$  in the complex plane to be inside a particular region of the interval. A method to evaluate the interval probability consists in taking into account the area covered by the overall interval array factor and a portion of it.

To compute the probability, one can follow these steps:

- *Step 1*: subdivision of the interval into regions.
- *Step 2*: computation of the probability for each region.
- *Step 3*: computation of the region bounds for the interval power pattern.

In the following each step will be better explained.

*Step 1*: For each angular direction, the interval bounds  $|AF_{inf}(u)|$  and  $|AF_{sup}(u)|$  can be considered the inner and outer radius of a circular ring  $\mathcal{G}$ , containing the interval phasor  $[AF(u)]$  (Fig. 2). Its width can be easily computed as  $w = w([AF(u)]) = |AF_{sup}(u)| - |AF_{inf}(u)|$ . It is possible to subdivide the ring  $\mathcal{G}$  into a certain number of sub-regions with equal width ( $w_\sigma$ ). In particular let us suppose to partition  $\mathcal{G}$  and as consequence  $[AF(u)]$  into  $K$  regions ( $\mathcal{G}_k$ ,  $[AF^k(u)]$ ,  $k = 1, \dots, K$ ) of equal width  $w_\sigma$  (Fig. 3):

$$w_\sigma = w([AF^k(u)]) = \frac{w}{K}, \quad k = 1, \dots, K \quad (6)$$

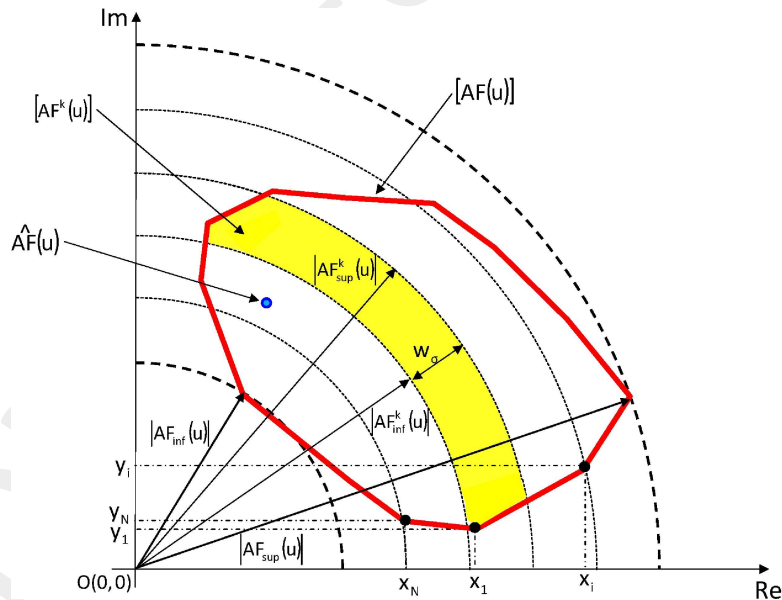


Figure 3: Subdivision of the interval array factor into  $K$  regions,  $[AF^k(u)]$ ,  $k = 1, \dots, K$ .

Therefore, for each region, the upper and lower endpoints are given by:

$$\begin{aligned} [AF^k(u)] &= [ |AF_{inf}^k(u)|, |AF_{sup}^k(u)| ] \\ &= [ |AF_{inf}(u)| + (k-1)w_\sigma, |AF_{sup}(u)| + kw_\sigma ], \quad k = 1, \dots, K \end{aligned} \quad (7)$$

It can be noticed that the lower and upper bounds of the  $K$  regions ( $[AF^k(u)]$ ,  $k = 1, \dots, K$ ) define a series of  $K + 1$  concentric circles ( $\mathcal{C}_k$ ,  $k = 1, \dots, K + 1$ ), having as center the origin of the complex plane  $O(0, 0)$ . In particular,  $\mathcal{C}_1$  has radius  $r_1 = |AF_{inf}(u)|$  and  $\mathcal{C}_{K+1}$  has radius  $r_{K+1} = |AF_{sup}(u)|$  and they are respectively the inner circumference ( $\mathcal{C}_1$ ) and the outer circumference ( $\mathcal{C}_{K+1}$ ) of the ring  $\mathcal{G}$ . Considering the  $K + 1$  concentric circumferences, the complex plane results subdivided into  $K$  annular regions ( $\mathcal{G}_k$ ,  $k = 1, \dots, K$ ) where the  $k$ -th ring has inner radius equal to  $r_k = |AF_{inf}^k(u)|$ ,  $k = 1, \dots, K$  and outer radius equal to  $r_{k+1} = |AF_{sup}^k(u)|$ ,  $k = 1, \dots, K$  (Fig. 4).

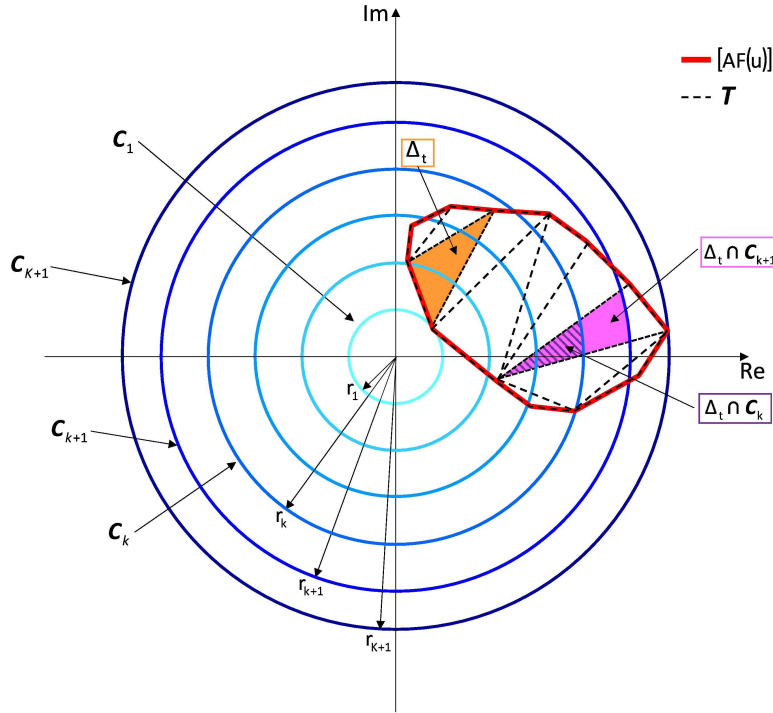


Figure 4: Sketch of the  $K$  annular regions in the complex plane, given  $K + 1$  concentric circumferences,  $[AF(u)]$  (red line), its triangulation  $\mathcal{T}$  (black dashed line) and an example of computation of the area given a triangle  $\Delta_t$ .

*Step 2:* The probability for a given array factor sample  $\hat{AF}(u)$  to belong to  $k$ -th region can be calculated as:

$$p_k(u) = \Pr \left\{ \hat{AF}(u) \in [AF^k(u)] \right\} = \frac{\mathcal{A}([AF^k(u)])}{\mathcal{A}([AF(u)])} \quad k = 1, \dots, K \quad (8)$$

where  $\mathcal{A}([AF^k(u)])$  is the area of the  $k$ -th portion of the interval array factor and  $\mathcal{A}([AF(u)])$  is the overall area of the interval array factor. To calculate the areas, one can adopt these steps:

- *Step 2.1:* To compute  $\mathcal{A}([AF(u)])$ , it is possible to use the so-called *Shoelace Algorithm (Gauss's area formula)*, a mathematical algorithm to determine the area of a simple polygon in a 2D plane given its  $N$  vertexes in cartesian coordinates (Fig. 3):

$$\begin{aligned} \mathcal{A}([AF(u)]) &= \frac{1}{2} \left| \sum_{i=1}^{N-1} x_i y_{i+1} + x_N y_1 - \sum_{i=1}^{N-1} x_{i+1} y_i - x_1 y_N \right| \\ &= \frac{1}{2} |x_1 y_2 + x_2 y_3 + \dots + x_{N-1} y_N + x_N y_1 - x_2 y_1 - x_3 y_2 - \dots - x_N y_{N-1} - x_1 y_N| \quad (9) \end{aligned}$$

being  $(x_i, y_i)$  with  $i = 1, \dots, N$  the  $i$ -th vertex of the polygon. The vertexes have been considered in anticlockwise

order, starting from the one with the smallest  $y$ -coordinate.

- *Step 2.2:* The computation of the area of the  $k$ -th region,  $[AF^k(u)]$  is more complex. It can be shown that each ring  $\mathcal{G}_k$ ,  $k = 1, \dots, K$ , previously defined, contains a portion of the interval array factor  $[AF(u)]$  (Fig. 4). In order to calculate the area covered by  $[AF^k(u)]$ , it is possible to exploit the triangulation  $\mathcal{T}$  of  $[AF(u)]$ .

Let us suppose that  $\mathcal{T}$  is constituted by  $T$  triangles (i.e.  $\mathcal{T} = \{\Delta_t, t = 1, \dots, T\}$ ), the area  $\mathcal{A}([AF^k(u)])$  can be calculated as a difference between the portion of  $[AF(u)]$  inside the upper circle  $\mathcal{C}_{k+1}$  and the portion of  $[AF(u)]$  inside the lower circle  $\mathcal{C}_k$ , thus obtaining the portion of  $[AF(u)]$  inside  $\mathcal{G}_k$ :

$$\begin{aligned}\mathcal{A}([AF^k(u)]) &= \mathcal{A}(\mathcal{T} \cap \mathcal{G}_k) \\ &= \mathcal{A}(\mathcal{T} \cap \mathcal{C}_{k+1}) - \mathcal{A}(\mathcal{T} \cap \mathcal{C}_k), \quad k = 1, \dots, K\end{aligned}\tag{10}$$

where  $\mathcal{A}(\mathcal{T} \cap \mathcal{C}_{k+1})$  and  $\mathcal{A}(\mathcal{T} \cap \mathcal{C}_k)$  are the areas of the portion of triangles inside the  $(k+1)$ -th circle and the  $k$ -th circle, respectively. The symbol  $\cap$  denotes the intersection between sets of points. The areas are determined as follows:

$$\begin{cases} \mathcal{A}(\mathcal{T} \cap \mathcal{C}_{k+1}) = \sum_{t=1}^T \mathcal{A}(\Delta_t \cap \mathcal{C}_{k+1}) \\ \mathcal{A}(\mathcal{T} \cap \mathcal{C}_k) = \sum_{t=1}^T \mathcal{A}(\Delta_t \cap \mathcal{C}_k) \end{cases} \quad k = 1, \dots, K\tag{11}$$

where  $\mathcal{A}(\Delta_t \cap \mathcal{C}_{k+1})$  and  $\mathcal{A}(\Delta_t \cap \mathcal{C}_k)$  are computed analysing the mutual position of the  $t$ -th triangle  $\Delta_t$  with respect to the circumference  $\mathcal{C}_k$ .

More in details, let us consider a triangle  $\Delta_t = \{v_j, j = 1, \dots, 3\}$ , being  $v_j, j = 1, \dots, 3$  the triangle vertexes in anticlockwise order. Moreover, let us call  $e_j, j = 1, \dots, 3$  the triangle edges. Analysing the position of both vertexes and edges with respect to a given circle  $\mathcal{C}_k$ , the area  $\mathcal{A}(\Delta_t \cap \mathcal{C}_k)$  can be computed according to the following procedure. In particular, the computation of the area can be realised as a summation or subtraction of three main subroutines, evaluating the area of three different geometrical shapes:

- $F_1 = \mathcal{A}(\mathcal{P})$  where  $\mathcal{P}$  is a simple polygon with  $P$  vertexes,
- $F_2 = \mathcal{A}(\mathcal{C})$  where  $\mathcal{C}$  is a circle,
- $F_3 = \mathcal{A}(\mathcal{S})$  where  $\mathcal{S}$  is a circular segment.

Let us now classify the different cases, according to the vertexes position with respect to the circle:

1. No vertexes inside the circle,  $v_j \notin \mathcal{C}_k, j = 1, \dots, 3$ , analysing the edges different area computations must be performed:

(a) No edges intersect the circumference:  $e_j \cap \mathcal{C}_k = \emptyset \forall j = 1, \dots, 3$

This is a trivial case and generates two opposite sub-cases in terms of result area:

- i. The origin of the complex plane does not lie inside the triangle:  $O(0, 0) \notin \Delta_t : \mathcal{A}(\Delta_t \cap \mathcal{C}_k) = 0$ , the area is null.
- ii. The origin of the complex plane lies inside the triangle:  $O(0, 0) \in \Delta_t : \mathcal{A}(\Delta_t \cap \mathcal{C}_k) = F_2 = \mathcal{A}(\mathcal{C}_k)$ , the area is the one of the whole circle.

(b) One edge intersects the circumference: let us suppose that edge  $e_1$  intersects the circumference  $\mathcal{C}_k$  in two points  $a_1$  and  $a_2$ :  $e_1 \cap \mathcal{C}_k = \{a_1, a_2\}$ . The area  $\mathcal{A}(\Delta_t \cap \mathcal{C}_k) = F_3 = \mathcal{A}(\mathcal{S}_1)$ , being  $\mathcal{S}_1$  the circular segment delimited by the chord and the circular arc having as extreme points  $a_1$  and  $a_2$ .

(c) Two edges intersect the circumference: let us suppose that the edges  $e_1$  and  $e_2$  intersect the circumference in  $e_1 \cap \mathcal{C}_k = \{a_1, a_2\}$  and in  $e_2 \cap \mathcal{C}_k = \{a_3, a_4\}$ . The two couples of intersecting points define two circular segments  $\mathcal{S}_1$  and  $\mathcal{S}_2$ , having as chord the part of edge between points  $a_1, a_2$  and  $a_3, a_4$ , respectively. Thus, the computation of the area involves the subtraction of the areas computed by two subroutines:  $\mathcal{A}(\Delta_t \cap \mathcal{C}_k) = F_2 - F_3 = \mathcal{A}(\mathcal{C}_k) - [\mathcal{A}(\mathcal{S}_1) + \mathcal{A}(\mathcal{S}_2)]$ .

(d) Three edges intersect the circumference: let us suppose that each edge  $e_j, j = 1, \dots, 3$  intersect the circumference in  $e_1 \cap \mathcal{C}_k = \{a_1, a_2\}$ ,  $e_2 \cap \mathcal{C}_k = \{a_3, a_4\}$  and  $e_3 \cap \mathcal{C}_k = \{a_5, a_6\}$ . As for the previous case, each couple of intersecting points defines three circular segments  $\mathcal{S}_1, \mathcal{S}_2$  and  $\mathcal{S}_3$ , having as chord the part of edge between points  $a_1, a_2, a_3, a_4$  and  $a_5, a_6$ , respectively. The computation of the area follows the same line of reasoning of the previous case:  $\mathcal{A}(\Delta_t \cap \mathcal{C}_k) = F_2 - F_3 = \mathcal{A}(\mathcal{C}_k) - [\mathcal{A}(\mathcal{S}_1) + \mathcal{A}(\mathcal{S}_2) + \mathcal{A}(\mathcal{S}_3)]$ .

2. One vertex inside the circle, analysing the edges two sub-cases can be distinguished:

(a) two edges intersect the circumference: let us suppose that  $v_1 \in \mathcal{C}_k$  and therefore,  $e_1$  and  $e_3$  intersect the circumference respectively in  $e_1 \cap \mathcal{C}_k = \{a_1\}$  and  $e_3 \cap \mathcal{C}_k = \{a_2\}$ . To compute the area two subroutines must be used:  $\mathcal{A}(\Delta_t \cap \mathcal{C}_k) = F_1 + F_3 = \mathcal{A}(\mathcal{P}) + \mathcal{A}(\mathcal{S}_1)$ , where  $\mathcal{P}$  is a polygon with  $P = 3$  vertexes:

- $\mathcal{P} = \{v_1, a_1, a_2\}$  sorted in anticlockwise order, and  $\mathcal{S}_1$  is a circular segment, having as chord the line joining the points  $a_1, a_2$ .
- (b) three edges intersect the circumference: let us suppose that  $v_1 \in \mathcal{C}_k$  and that each edge  $e_j, j = 1, \dots, 3$  intersects the circumference in  $e_1 \cap \mathcal{C}_k = \{a_1\}, e_2 \cap \mathcal{C}_k = \{a_2, a_3\}$  and  $e_3 \cap \mathcal{C}_k = \{a_4\}$ . Similarly as the previous case,  $\mathcal{A}(\Delta_t \cap \mathcal{C}_k) = F_1 + F_3 = \mathcal{A}(\mathcal{P}) + \mathcal{A}(\mathcal{S}_1) + \mathcal{A}(\mathcal{S}_2)$ , where  $\mathcal{P}$  is a polygon with  $P = 5$  vertexes,  $\mathcal{P} = \{v_1, a_1, a_2, a_3, a_4\}$ , in anticlockwise order, while  $\mathcal{S}_1$  and  $\mathcal{S}_2$  are two circular segments, having as chord the line joining the points  $a_1, a_2$  and  $a_3, a_4$ , respectively.
3. Two vertexes inside the circle: let us suppose that  $v_1, v_2 \in \mathcal{C}_k$ , and as consequence edge  $e_1$  entirely lies inside the circle, too. Instead, edges  $e_2$  and  $e_3$  must intersect the circumference respectively in  $e_2 \cap \mathcal{C}_k = \{a_1\}$  and  $e_3 \cap \mathcal{C}_k = \{a_2\}$ . The area can be compute in the following way:  $\mathcal{A}(\Delta_t \cap \mathcal{C}_k) = F_1 + F_3 = \mathcal{A}(\mathcal{P}) + \mathcal{A}(\mathcal{S}_1)$ , where  $\mathcal{P}$  is a polygon with  $P = 4$  vertexes,  $\mathcal{P} = \{v_1, v_2, a_1, a_2\}$  in anticlockwise order and  $\mathcal{S}_1$  is a circular segment, having as chord the line joining the points  $a_1, a_2$ .
4. Three vertexes inside the circle: this case is a trivial since  $\mathcal{A}(\Delta_t \cap \mathcal{C}_k) = \mathcal{A}(\mathcal{P})$ , where  $\mathcal{P}$  is the triangle itself  $\mathcal{A}(\mathcal{P}) = \mathcal{A}(\Delta_t)$ .

This procedure must be repeated for all the  $T$  triangles against the  $K + 1$  circumferences.

Notice that, the hypothesis introduced during the procedure explanation have been done only for sake of simplicity.

*Step 3:* For each region, the power pattern  $[P^k(u)]$ ,  $k = 1, \dots, K$  can be calculated starting from the corresponding array factor region  $[AF^k(u)]$ ,  $k = 1, \dots, K$ , in the following way:

$$\begin{aligned} [P^k(u)] &= [P_{inf}^k(u), P_{sup}^k(u)] \\ &= \left[ |AF_{inf}^k(u)|^2, |AF_{sup}^k(u)|^2 \right] \quad k = 1, \dots, K \end{aligned} \quad (12)$$

Finally, given  $H$  angular direction and knowing that the probability of each power pattern region  $[P^k(u)]$ ,  $k = 1, \dots, K$  is equal to the probability of each array factor region  $[AF^k(u)]$  for definition, one can also compute the mean probability of each power pattern region ( $\bar{p}_k$ ):

$$\bar{p}_k = \frac{1}{H} \sum_{h=1}^H p_k(u_h) \quad k = 1, \dots, K \quad (13)$$

---

## Probabilistic Interval Analysis - Power Pattern Features

To better quantify the effects of the excitations tolerance on the array radiation properties, the interval related to  $[SLL]$ ,  $[HPBW]$  and  $[P_{max}]$  have been computed for the IA-MS bounds.

However, these power pattern features should now be customised for each array factor region  $[AF^k(u)]$ ,  $k = 1, \dots, K$ . More in details, for each region  $[AF^k(u)]$ ,  $k = 1, \dots, K$  the worst achievable sidelobe level ( $SLL_k^{worst}$ ,  $k = 1, \dots, K$ ) and the worst possible half-power beamwidth ( $HPBW_k^{worst}$ ,  $k = 1, \dots, K$ ) have been defined as:

$$SLL_k^{worst} = \max_{u \notin \Omega} \{P_{sup}^k(u)\} - \max_{u \in \Omega} \{P_{inf}^k(u)\} \quad k = 1, \dots, K \quad (14)$$

$$HPBW_k^{worst} = u_{3dB,r} - u_{3dB,l} \quad k = 1, \dots, K \quad (15)$$

where  $u_{3dB,l} = \min\{u : P_{inf}^k(u) = P_{inf}^k(u) - 3[\text{dB}]\}$  and  $u_{3dB,r} = \max\{u : P_{inf}^k(u) = P_{inf}^k(u) - 3[\text{dB}]\}$  are the angular directions in correspondence with the two points of  $P_{sup}(u)$  having a power 3 [dB] below  $\max_{u \in \Omega} \{P_{inf}^k(u)\}$ .

Moreover, for each interval region also the maximum power pattern interval  $[P_{max}^k]$ ,  $k = 1, \dots, K$  and the Normalised Power Pattern Matching  $\Delta_n^k$ ,  $k = 1, \dots, K$  have been defined:

$$[P_{max}^k] = \begin{cases} P_{max}^{inf,k} = \max_{u \in \Omega} \{P_{inf}^k(u)\} \\ P_{max}^{sup,k} = \max_{u \in \Omega} \{P_{sup}^k(u)\} \end{cases} \quad k = 1, \dots, K \quad (16)$$

$$\Delta_n^k = \frac{\int_{-1}^{+1} (P_{sup}^k(u) - P_{inf}^k(u)) du}{\int_{-1}^{+1} |AF(u)|^2 du} \quad k = 1, \dots, K \quad (17)$$

---

More information on the topics of this document can be found in the following list of references.

## References

- [1] P. Rocca, N. Anselmi, A. Benoni, and A. Massa, "Probabilistic interval analysis for the analytic prediction of the pattern tolerance distribution in linear phased arrays with random excitation errors," *IEEE Trans. Antennas Propag.*, vol. 68, no. 2, pp. 7866-7878, Dec. 2020.
- [2] L. Tenuti, N. Anselmi, P. Rocca, M. Salucci, and A. Massa, "Minkowski sum method for planar arrays sensitivity analysis with uncertain-but-bounded excitation tolerances" *IEEE Trans. Antennas Propag.*, vol. 65, no. 1, pp. 167-177, Jan. 2017.
- [3] N. Anselmi, P. Rocca, M. Salucci, and A. Massa, "Optimization of excitation tolerances for robust beamforming in linear arrays," *IET Microwaves, Antennas & Propagation*, vol. 10, no. 2, pp. 208-214, 2016.
- [4] N. Anselmi, P. Rocca, M. Salucci, and A. Massa, "Power pattern sensitivity to calibration errors and mutual coupling in linear arrays through circular interval arithmetics," *Sensors*, vol. 16, no. 6 (791), pp. 1-14, 2016.
- [5] L. Poli, P. Rocca, N. Anselmi, and A. Massa, "Dealing with uncertainties on phase weighting of linear antenna arrays by means of interval-based tolerance analysis," *IEEE Trans. Antennas Propag.*, vol. 63, no. 7, pp. 3299-3234, Jul. 2015.
- [6] P. Rocca, N. Anselmi, and A. Massa, "Optimal synthesis of robust array configurations exploiting interval analysis and convex optimization," *IEEE Trans. Antennas Propag.*, vol. 62, no. 7, pp. 3603-3612, July 2014.
- [7] T. Moriyama, L. Poli, N. Anselmi, M. Salucci, and P. Rocca, "Real array pattern tolerances from amplitude excitation errors," *IEICE Electronics Express*, vol. 11, no. 17, pp. 1-8, Sep. 2014.
- [8] N. Anselmi, L. Manica, P. Rocca, and A. Massa, "Tolerance analysis of antenna arrays through interval arithmetic," *IEEE Trans. Antennas Propag.*, vol. 61, no. 11, pp. 5496-5507, Nov. 2013.
- [9] L. Manica, N. Anselmi, P. Rocca, and A. Massa, "Robust mask-constrained linear array synthesis through an interval-based particle swarm optimisation," *IET Microwaves, Antennas and Propagation*, vol. 7, no. 12, pp. 976-984, Sep. 2013. P. Rocca, L. Manica, N. Anselmi, and A. Massa, "Analysis of the pattern tolerances in linear arrays with arbitrary amplitude errors," *IEEE Antennas Wireless Propag. Lett.*, vol. 12, pp. 639-642, 2013.
- [10] L. Manica, P. Rocca, N. Anselmi, and A. Massa, "On the synthesis of reliable linear arrays through interval arithmetic," *IEEE International Symposium on Antennas Propag. (APS/URSI 2013)*, Orlando, Florida, USA, Jul. 7-12, 2013.
- [11] L. Manica, P. Rocca, G. Oliveri, and A. Massa, "Designing radiating systems through interval analysis tools," *IEEE International Symposium on Antennas Propag. (APS/URSI 2013)*, Orlando, Florida, USA, Jul. 7-12, 2013.

- 
- [12] M. Carlin, N. Anselmi, L. Manica, P. Rocca, and A. Massa, "Exploiting interval arithmetic for predicting real arrays performances - The linear case," IEEE International Symposium on Antennas Propag. (APS/URSI 2013), Orlando, Florida, USA, Jul. 7-12, 2013.
- [13] N. Anselmi, M. Salucci, P. Rocca, and A. Massa, "Generalized sensitivity analysis tool for pattern distortions in reflector antennas with bump-like surface deformations," IET Microwaves, Antennas & Propagation, vol. 10, no. 9, p. 909-916, June 2016.
- [14] P. Rocca, L. Poli, N. Anselmi, M. Salucci, and A. Massa, "Predicting antenna pattern degradations in microstrip reflectarrays through interval arithmetic," IET Microwaves, Antennas & Propagation, vol. 10, no. 8, pp. 817-826, May 2016.
- [15] P. Rocca, L. Manica, and A. Massa, "Interval-based analysis of pattern distortions in reflector antennas with bump-like surface deformations," IET Microwaves, Antennas and Propagation, vol. 8, no. 15, pp. 1277-1285, Dec. 2014.
- [16] P. Rocca, N. Anselmi, and A. Massa, "Interval Arithmetic for pattern tolerance analysis of parabolic reflectors," IEEE Trans. Antennas Propag., vol. 62, no. 10, pp. 4952-4960, Oct. 2014.
- [17] P. Rocca, M. Carlin, L. Manica, and A. Massa, "Microwave imaging within the interval analysis framework," Progress in Electromagnetic Research, vol. 143, pp. 675-708, 2013.
- [18] L. Manica, P. Rocca, M. Salucci, M. Carlin, and A. Massa, "Scattering data inversion through interval analysis under Rytov approximation," 7th European Conference on Antennas Propag. (EuCAP 2013), Gothenburg, Sweden, Apr. 8-12, 2013.
- [19] P. Rocca, M. Carlin, and A. Massa, "Imaging weak scatterers by means of an innovative inverse scattering technique based on the interval analysis," 6th European Conference on Antennas Propag. (EuCAP 2012), Prague, Czech Republic, Mar. 26-30, 2012.
- [20] P. Rocca, M. Carlin, G. Oliveri, and A. Massa, "Interval analysis as applied to inverse scattering," IEEE International Symposium on Antennas Propag. (APS/URSI 2013), Chicago, Illinois, USA, Jul. 8-14, 2012.